MOLECULAR EVIDENCE OF LATE ARCHEAN ARCHAEA AND THE PRESENCE OF A SUBSURFACE HYDROTHERMAL BIOSPHERE

Gregory T. Ventura[1*], Fabien Kenig[1], Christopher M. Reddy[2], Juergen Schieber[3], Glenn S. Frysinger[4], Robert K. Nelson[2], Etienne Dinel[5], Richard B. Gaines[4], Philippe Schaeffer[6]

[1] Department of Earth and Environmental Sciences, University of Illinois at Chicago, M/C 186, 845 West Taylor Street, Chicago IL 60607-7059, USA.

[2] Department of Marine Chemistry and Geochemistry, MS#4, Woods Hole Oceanographic Institution, Woods Hole, MA 02543-1543, USA.

[3] Department of Geological Sciences, 1001 East 10th Street, Indiana University, Bloomington, IN. 47405-1405, USA.

[4] Department of Science, 310 Smith Hall, U.S. Coast Guard Academy, New London, CT 06320-8101, USA.

[5] Earth Sciences Department, Ottawa-Carleton Geoscience Centre, University of Ottawa, Ottawa, Ontario, Canada, K1N 6N5.

[6] Laboratoire de Géochimie Bio-organique, UMR 7509 du CNRS, Ecole de Chimie, Polymères et Matériaux, Université Louis Pasteur, 25 rue Becquerel, 67200 Strasbourg, France.

Conflict of Interest Statement: No conflicts declared.

Abbreviations: Ma, million years old; PGC, Porcupine Gold Camp; HPCH, high pressure catalytic hydrogenation; UCM, unresolved complex mixture; GDGT, glycerol dibiphytanyl glycerol tetraether; PDB, Pee Dee belemnite; GC×GC, comprehensive two dimensional gas chromatography.

Author contributions: G.T.V. and F.K. designed research and wrote the paper, G.T.V. performed research, J.S. designed petrographic study, C.M.R., G.F., R.K.N. and R.B.G., GC×GC support; P.S. and E.D. provided technical support.

* to whom correspondence should be sent.

Abstract

Highly cracked and isomerized archaeal lipids and bacterial lipids, structurally changed by thermal stress, are present in solvent extracts of 2,707-2,685 million year old (Ma) metasedimentary rocks from Timmins, Ontario, Canada. These lipids appear in conventional gas chromatograms as unresolved complex mixtures (UCMs) and include cyclic and acyclic biphytanes, C_{36}-C_{39} derivatives of the biphytanes, and C_{31}-C_{35} extended hopanes. Biphytane and extended hopanes are also found in high pressure catalytic hydrogenation (HPCH) products released from solvent-extracted sediments,

indicating that archaea and bacteria were present in Late Archean sedimentary environments. Post-depositional, hydrothermal gold mineralization and graphite precipitation occurred prior to metamorphism (~2,665 Ma). Late Archean metamorphism significantly reduced the kerogen's adsorptive capacity and severely restricted sediment porosity, limiting the potential for post-Archean additions of organic matter to the samples. Argillites exposed to hydrothermal gold mineralization have disproportionately high concentrations of extractable archaeal and bacterial lipids relative to what is releasable from their respective HPCH product and what is observed for argillites deposited away from these hydrothermal settings. The addition of these lipids to the sediments likely results from a Late Archean subsurface hydrothermal biosphere of archaea and bacteria.

1. Introduction

An early evolution of archaea is supported by the discovery of ^{13}C-depleted methane in ~3,500 Ma hydrothermal fluid inclusions in cherts from the Pilbara Craton of Australia (1). In the Late Archean, archaea are likely to have played a dominant role in the global carbon cycle. Kerogens with δ^{13}C values down to -60‰ *vs* VPDB are common between 2,800 and 2,600 Ma (2, 3). These are considered to have formed by the burial of methanotrophs or other organisms that assimilated ^{13}C-depleted carbon resulting from isotopic fractionations during methanogenesis (4). Biogenic methane not immediately assimilated is thought to have entered the atmosphere (5), enhanced greenhouse warming

and offset the reduced insolation from a "faint" young sun (6). As such, archaea were indirectly responsible for the existence of liquid water at the earth's surface.

In more recent sediments, the presence of archaea is inferred from isotopic evidence of methane cycling (7, 8) or by detection of domain-specific membrane lipids such as glycerol dibiphytanyl glycerol tetraethers (GDGTs) (9) or their degradation products (10). The oldest known GDGTs (11) and biphytane-derived, C_{39} head-to-head isoprenoids (12) occur in Upper Jurassic sediments and in crude oil, respectively. The archaeal lipid crocetane was tentatively identified in 1,640 Ma sediments from the Barney Creek Formation (13).

In principle, it should be possible to extend this record. Petroleum fluid inclusions, bitumen globules, and pyrobitumens occur in 3,200-2,440 Ma black shales of the Pilbara Craton, Australia (14-16). Migrated hydrocarbons of Archean age have been identified in the Witwatersrand Basin of South Africa (17). Molecular fossils diagnostic of bacteria and eukarya have been extracted from 2,700 Ma sediments of the Hammersley Basin of Western Australia and provide direct evidence for a Late Archean existence of these two domains of life (18). Hydrothermal settings may further enhance the potential for Archean molecular fossils to survive because high pressure and temperature aqueous solutions suppress the thermal destruction of hydrocarbons (19).

This investigation was conducted to assess the abundance and preservation of molecular fossils within Late Archean hydrothermal environments and hydrothermally altered sediments. Samples were collected from the lower greenschist metasediments (20, 21) of the Tisdale and Porcupine Assemblage (~2,707-2,685 Ma) from the southern Abitibi greenstone belt near Timmins, Ontario, Canada. Here we report the occurrence of

hydrocarbon molecular fossils diagnostic of archaea and bacteria among the solvent-extractable lipids and HPCH products (22) of these samples. We provide evidence that these lipids are of Archean age and that a portion of the organic matter trapped in these sediments was derived from a subsurface hydrothermal biosphere.

2. Results and Discussion

Thirty samples were collected from the core library of the Ministry of Northern Development and Mines, as well as from the Dome, Hoyle Pond, and Owl Creek mines located in the Porcupine Gold Camp (PGC), a gold mine district. These samples span the Vipond and Gold Center Formations of the upper Tisdale Assemblage (2,710-2,704 Ma) and the Krist and Hoyle Formation of the Porcupine Assemblage (2,690-2,685 Ma; Fig. 1) (23). The Vipond Formation volcanic rocks range in composition from mafic to intermediate and from tholeiitic basalt to tholeiitic dacite interbedded by interflow sedimentary rocks (24). Four different interflow sedimentary units of greywacke and carbonaceous argillites were analyzed. Two samples of carbonaceous interflow sediments were analyzed from the overlying Gold Center Formation. These sediments were deposited between mafic pillowed flows, pillow breccias and flow breccias. One sample of a sheared, carbonaceous argillite from the Krist Formation was analyzed. The Krist Formation is dominated by subaerially deposited calc-alkaline felsic pyroclastic volcanic rocks (24). Nineteen core samples were collected from argillites and wackes of the Hoyle Formation, which consists of turbidites interbedded between basalt flows on the distal,

deeper-water margin of a submarine fan system (25). Two of these samples occupied "grey zones", which are volcanic breccia enriched in graphite, pyrite, dolomite, and ferroan-dolomite precipitated by hydrothermal gold-bearing fluids (26). Grey zones cross-cut volcanic rock, argillaceous turbidites, and interflow sedimentary units. Additionally, four interbedded basalt flows were sampled to monitor post-depositional alteration and contamination. The Porcupine Assemblage is unconformably topped by fault-controlled, clastic sediments of the Timiskaming Sequence that range from 2,676-2,670 Ma (27). No other sedimentary units are known from this area. By 2,670 ±7 Ma the Porcupine Assemblage was a site of hydrothermal gold mineralization (28). The PGC was metamorphosed at 200-300ºC between 2,669-2,665 Ma (20, 21, 29).

Polished thin sections (30 and 100-µm) were analyzed by scanning electron microscopy. The Vipond Formation samples contain wavy-laminar, carbon-rich films adjacent to sedimentary sulfides (Fig. 2A). Additionally, carbon-rich inclusions were identified within these greywackes. These inclusions occur as fillings in ~1-µm wide cracks between and adjacent to pyrite grains (Fig. 2B and C); as ~10-20-µm diameter, rounded inclusions within the interstices of occluded quartz grains (Fig. 2C); and as ~10-20-µm diameter, rounded, carbon-rich inclusions within secondary mineral phases such as ferroan-dolomite (Fig. 2D and E). The large (~100-300-µm) ferroan-dolomite grains formed during precipitation of minerals from hydrothermal fluids (30) and contain rounded inclusions of apatite and quartz. Iron-enriched halos surrounding quartz and carbon-rich inclusions (Fig. 2D and E) indicate these spaces were likely filled by a hydrocarbon-bearing fluid that later became solid bitumen prior to quartz deposition.

The fine-grained, meta-sedimentary fabric of samples from the Hoyle Formation contains laminae with carbon-rich films that contain bitumen and kerogen (Fig. 2F and G). No carbon-rich inclusions were observed. Many of the fine-grained matrix sulfides are flanked by quartz-filled pressure shadows (Fig. 2H), suggesting the remobilization of quartz during prograde metamorphism. In all stratigraphic sections, the initial sediment porosity was occluded by remobilized quartz and by the growth of potassium and aluminum silicate (Fig. 2H). Conversion to slate resulted in the formation of dense, non-porous rock that is impermeable to post-metamorphic fluids and/or migrating oils. There is no evidence of post-Archean remineralization or retrograde metamorphic alteration that could trap more recent contributions of organic matter.

2.1. Organic Carbon and Graphite

All PGC samples have hydrogen to carbon ratios less than 0.2 (Table 1). Hoyle Formation samples collected from areas of gold mineralization have near-zero hydrogen to carbon ratios (Table 1). The coexistence of saturated hydrocarbons and nearly graphitic kerogen could suggest a post-metamorphic addition of hydrogen-rich organic compounds. However, if factors other than thermal stress influence the concentrations of hydrogen and carbon of sedimentary organic matter, then, H/C ratios are not a reliable proxy of hydrocarbon preservation.

The PGC experienced extensive carbonatization prior to metamorphism (Fig. 3) (30). Fluid with high CO_2 fugacity induced precipitation of carbonates in less reducing settings (31) and graphite in more reducing environments. Exogenous additions of

graphite are common in the PGC gold centers (24) and globally observed in hydrothermal load-gold deposits (32-34). Additions of graphite

$$n\ CO_{2\ (mantle)} + (2n+x)\ CH_2 \rightarrow 3n\ C^0 + 2n\ H_2O + x\ CH_{2\ (hydrothermally\ altered)}$$

(rather than generation of graphite in situ by dehydrogenation and aromatization of kerogen) can explain the coexistence of hydrocarbons with kerogens having near-zero H/C ratios. The addition of hydrothermal graphite also accounts for the slightly more positive values of $\delta^{13}C_{ker}$ of Hoyle Formation samples collected in areas of gold mineralization and the lack of correlation between H/C ratios, TOC, and bitumen extracted from the PGC sediments (Table 1).

2.2. Biphytanes in Bitumens

The solvent-extractable hydrocarbons of these powdered sediment samples were analyzed by gas chromatography-mass spectrometry (GCMS) [supporting information (SI) *Text*]. All but one sample contains biphytane and C_{36}-C_{39} irregular isoprenoids derived from biphytane (Fig. 1). These compounds were identified from their mass spectra and by coinjection with a standard containing acyclic, mono-, bi-, and tricyclic biphytanes (SI Fig. 1). The abundances of biphytanes relative to other extractable compounds vary between and within formations. Hoyle Formation samples located away from gold mineralization centers have low concentrations of biphytanes and extended hopanes. In contrast, those compounds and their degradation products are among the most abundant compounds in the solvent-extractable hydrocarbons of samples collected

in areas of gold mineralization (Fig. 1). Only the sample of the Krist Formation does not contain archaeal lipids.

2.3. Archaeal Lipids of Unresolved Complex Mixtures

Gas chromatograms of hydrocarbon extracts of samples collected in areas of gold mineralization display discrete peaks of biphytane and related degradation products that elute within a pronounced UCM (Fig. 1). Bacterial biomarkers such as C_{27}-C_{35} hopanoid hydrocarbons and eukaryotic biomarkers such as C_{27}-C_{29} steroids were identifiable by GCMS but most of the constituents the UCMs remain undetermined.

Comprehensive two-dimensional gas chromatography coupled to a time-of-flight mass spectrometer (GC×GC-TOFMS) was used to resolve and identify the components forming the UCMs of the Hoyle Formation (*SI Text*) (Fig. 1). As shown in Figure 4, the constituents of the UCM are separated into bands of peaks with different retention times in the second dimension. The constituents of the first band are C_{36}-C_{41} head-to-head acyclic isoprenoids, including biphytane. The second, third, and fourth bands include, respectively, mono-, bi- and tricyclic biphytane and their derivatives (C_{36}-C_{39}). Tetracyclic triterpenoids (steroids) and pentacyclic triterpenoids (hopanoids) form a fifth and a sixth band in the second dimension.

The C_{40} mono, bi-, and tricyclic biphytane derivatives and their lower C_{36}-C_{39} pseudohomologues each form doublets, triplets, and at least quadruplets of peaks (Fig. 4), respectively, with identical mass spectra. In contrast, each of the C_{36}-C_{40} acyclic isoprenoids forms a single peak. With time and thermal stress, acyclic and cyclic biphytanes (35, 36) isomerize at methyl-substituted chiral carbons on the isoprenoid

chain (37) and at alkyl-substituted chiral carbon of pentacyclic rings. Although diastereomers formed by isomerization of acyclic compounds cannot be resolved with the GC×GC columns used (38), the doublets, triplets, and quadruplets observed for the cyclic compounds probably represent mixtures of diastereomers.

To date, the isomerization rate of such compounds under thermal stress is unknown. Although isomerization of acyclic isoprenoids is well established, a pattern of cyclic-isoprenoid diastereomers like that in the PGC samples has not been previously reported. The formation of such diastereomers must be favored by high temperatures and potentially requires the addition of metal catalysts (39) or exogenous sources of hydrogen to expand the activation energy range for isomerization without excessive hydrocarbon cracking (19). Such conditions might be common to hydrothermal environments where serpentinization and the hydrolytic disproportionation of H_2O forms solutions with high H_2 fugacity (19, 40, 41).

2.4. Potential for Bitumen Contamination

Sedimentary organic matter can be contaminated by post-burial addition of hydrocarbons. Potential sources include drilling fluids, laboratory processing, migration of oils, and infiltration by meteoric groundwater. Solvent washes of the core exterior contain abundant contaminants. Accordingly, the surfaces of cores were ground away before extraction. Solvent-washes conducted after the removal of the core surface contain only trace concentrations of the same hydrocarbons extracted from the powdered sediments (*SI Text*). Because these differ compositionally from the surface contaminants, we believe they do not derive from laboratory or field contamination. Analytical blanks

from solvent extraction and liquid chromatography have hydrocarbon contents 100 times smaller than those obtained from samples. In marked contrast to the significant differences between samples, replicate extraction of splits of a single sample yielded essentially identical mixtures of hydrocarbons. Solvent extracts of Hoyle Formation basalt units interstratifying the archaeal-rich turbidites do not contain archaeal lipids. However, these igneous rocks do have traces of hydrocarbons such as *n*-alkanes, pristane, and phytane (Fig. 1) attributable to rough storage and contamination by drilling fluids (*SI Text*).

The extractable hydrocarbons are unlikely to result from the migration of younger oils. The Vipond and Krist Formation samples were collected in ~3 m thick interflow deposits buried ~800 m beneath successive mafic flows within the Dome Mine. Hydrocarbon mixtures extracted from the Vipond and Krist Formations differ from those extracted from the Hoyle Formation. With allowance for the higher temperatures experienced at the PGC, the extracts of the Vipond and Krist Formations resemble those of younger hydrothermal settings and the extracts of the Hoyle Formation samples resemble those of younger shelf sediments (42, 43). In contrast, even though the depositional environment of the Gold Center Formation is similar to that of the Vipond and Krist Formations, its extracts have hydrocarbon abundances and diversities comparable to those from the overlying Hoyle Formation (Fig. 1) (*SI Text*). Migration from older units is not possible because these units are entirely igneous. Accordingly, the hydrocarbons may in part derive from the post-depositional addition of Late Archean oil migrated from source rocks in the Hoyle Formation.

2.5. High Pressure Catalytic Hydrogenation

The presence of archaeal- and bacterial-related lipid carbon skeletons in non-extractable organic matter is a strong indication that the lipids were part of the original sedimentary organic matter. HPCH can release lipid carbon skeletons from kerogen (44) and/or sulfides (22) trapped in metamorphosed sediments. Biphytane and C_{37}-C_{39} biphytane derivatives were observed in the HPCH products of all solvent-extracted sediment samples that contain extractable archaeal lipids (Fig. 5). Additionally, all HPCH products contain diasteranes, tricyclic terpanes and thermally altered steranes and hopanes. Several HPCH products have diasterane/sterane, sterane/hopanes, and tricyclic terpane/hopanes ratios that differ from those of their corresponding extracts, indicating these lipids were likely cracked from the kerogen (SI Table 3). However, the HPCH products of some samples include *n*-alkanes, monomethyl- and monoethyl-branched alkanes, as well as cycloalkanes with carbon-number predominance that is likely indicative of contamination during storage (45).

HPCH products can also derive from incomplete sediment extraction, molecules that are adsorbed on kerogen, and/or intercalated bitumen. Since re-extracted sediments yielded only extremely low abundances of lower molecular weight *n*-alkanes and elemental sulfur, we exclude incomplete extraction. Adsorption occurs mainly during early diagenesis and substantially decreases with increasing thermal maturity due to the loss of reactive sites on the kerogen (46). The PGC kerogens reached a thermal stress corresponding to the onset of metamorphism in the Late Archean (*SI Text*) and sediment porosity was significantly restricted thereafter. Any surviving, adsorbed organic matter, therefore, is Archean. The HPCH products may also contain intercalated bitumen, which

forms by the entrapment of bitumen in the kerogen during the continued heating of a thermally mature kerogen (47). Such constituents must be intimately associated with the kerogen, and, thus, also date from the Late Archean.

2.6. Second Addition of Archaeal and Bacterial Lipids

The presence of biphytane, steranes, and hopanes in the HPCH products indicates that all three domains of life were present in the Late Archean environment. However, the relative abundance of archaeal and bacterial products varies widely between samples. Specifically, archaeal and bacterial products are more abundant in sediments affected by gold mineralization (Fig. 5). Chromatograms on the left and right of Figure 5 represent unmineralized and mineralized areas, respectively. Similar relative abundances of these compounds in geographically and temporally separated turbidites of the Porcupine Formation suggest consistent sources, low in archaeal biomass, during sediment deposition (Fig. 5A, C). The abundance patterns of biphytane, biphytane derivatives, and C_{31}-C_{35} extended hopanes are similar in both the solvent extracts and HPCH products of samples collected away from gold mineralization centers. In these samples, the biphytane concentration in bitumen is typically low and uncorrelated to the sediment's total organic carbon (TOC) (Table 1). In contrast, within gold mineralization centers, biphytane and the C_{39} derivative of biphytane are often the most abundant molecular fossils in the solvent extracts and correlate positively with TOC. The relative abundances of biphytane, biphytane derivatives, and C_{31}-C_{35} extended hopanes in the solvent extracts are much greater than in the HPCH products of the corresponding samples (Fig. 5). Additionally, several samples with low TOC, such as the hydrothermally altered "grey zone" and

samples DP-1 and DP-2, have relatively high concentrations of biphytane and extended hopanes (*SI Text*), indicating that these lipids are unlikely to derive from cracking of kerogen and instead suggesting a secondary input of organic compounds.

Post-metamorphic hydrothermal activity is not likely to account for the secondary addition of organic matter. In the Southern Superior Province, it is linked to the 2,500 Ma Matachewan and 2,220 Ma Nipissing dyke swarms, the Trans-Hudson orogeny (~1,900 Ma), Kapuskasing uplift (1,900 Ma), and the Grenvillian Orogen (~1,100 Ma), which involved tectonic pumping of fluids in reactivated Archean fault systems (48) (Fig. 3). These fluids would have traveled ~100 kilometers before reaching the PGC. If such fluids added the archaeal biomarkers, then the basalt flows interstratifying the Hoyle Formation turbidites would also have been affected.

Alternatively, geochemical process relating to PGC gold mineralization may be responsible for variations in archaeal and bacterial lipid extract yields (Fig. 3). Gold is thought to have been transported within dilute, aqueous, carbonic fluids with low chlorine and high sulfur contents in the form of Au-HS^--complexes (49). Ore fluids were acidic (pH 5-6) and their redox properties were controlled by HSO_4/H_2S and CO_2/CH_4 mixtures at temperatures between 200-420ºC (48). Based on the solubility of Au-$(HS)^-$, gold precipitation is thought to have occurred at cooler temperatures and/or lower pressure (49). The envelope of cooled, high sulfur- and reduced, carbon-rich fluids surrounding this region of high heat flow would provide favorable conditions for hyperthermophilic communities of archaea and bacteria (50, 51). Continued burial would likely convert a subsurface biosphere's biomass into the observed secondary addition of hydrocarbons (Fig. 3).

3. Conclusions

A bacterial and archaeal subsurface biosphere is now believed to have a near-global extent, being found in marine sediments; in the fractures and vents near mid-oceanic spreading centers; within older, cooled basaltic crust beneath the oceans; in deep aquifers of basalts and granitic batholiths; and in deep oil reservoirs of continental settings (51-53). Our results provide molecular fossil evidence for the existence of archaea in Late Archean sedimentary environments and in subsurface hydrothermal settings. Considering the extent and composition of today's deep biosphere, it is likely that such hydrothermal subsurface communities have existed for much of earth history.

Materials and Methods:

Samples were collected from the core library of the Ministry of Northern Development and Mines, as well as from the Dome, Hoyle Pond, and Owl Creek mines operated by Porcupine Joint Ventures. Extraction, separation, HPCH protocols and instrumentation techniques are provided in the online supplemental information.

Acknowledgement:

We thank Porcupine Joint Venture and The Ministry of Northern Mines and Development (Ontario, Canada) for access to the gold mines and for samples. We also thank Eric Barr and the late Richard Keele for their help with sampling. We thank Roger Summons and Emmanuelle Grosjean (MIT), Neil Sturchio and Linnea Heraty (UIC) for sample analysis and Ben Van Mooy and Helen Fredricks (WHOI) for use of an internal

standard. Additionally, we thank John Hayes (WHOI) for invaluable editorial input. This project was supported by NASA Exobiology grant #NAG5-13446 to Fabien Kenig. SEM analysis was supported by NSF grant EAR 0318769 to Juergen Schieber. GC×GC analysis was supported by NSF grant IIS-0430835 and the Seaver Foundation to Christopher M. Reddy.

Figure 1. Stratigraphic profile of the Timmins area (left) and total ion current (TIC) chromatograms of samples (right) illustrating differences in the hydrocarbon fractions of each formation. UCM: unresolved complex mixture. Asterisk: samples collected in areas of gold mineralization. Double cross: Hoyle Formation basalt unit. Black circles: *n*-alkanes. H: hopanes. Open squares: biphytane and its derivatives.

Figure 2. (A) Transmitted light photomicrograph of the Vipond Formation greywacke sample DM-1. Opaque areas are sulfide minerals. (B and C) SEM backscatter images of carbon-rich inclusions (arrows). (D) Sample DM-1 SEM backscatter image of a carbon-rich inclusion (arrows) in Fe-dolomite. (E) Close-up of the carbon-rich inclusion. A Fe-enriched reduction-halo surrounds the partially quartz-filled inclusion. (F) Transmitted light photomicrograph of the Hoyle Formation argillite sample OC-114m. Original sedimentary lamination inclined 30º with horizontal slaty cleavage. (G) SEM backscatter image of Hoyle Formation sample OC-110m with carbon-rich films filling the interstices of quartz, muscovite, and Fe-dolomite grains. (H) Quartz-filled pressure shadows (arrows) flanking sulfide minerals. Abbreviations Apt, FD, Musc, Qtz, and Pyr are respectively apatite, Fe-dolomite, muscovite, quartz, and pyrite.

Figure 3. Time sequence of geological and geochemical events affecting the Porcupine Gold Complex modified from (54). Overlain on the hypothesized burial temperature curve are the temperature ranges of gold solubility (55), reduction of Au onto lignite (56), catagenesis and metagenesis (57), kerogen conversion to graphite (58), and stability of graphite in mixtures of CO_2 and CH_4 (59).

Figure 4. Three-dimensional GC×GC-FID chromatograms of the solvent extract from sample OC-114m of the Hoyle Formation. Bottom: complete chromatograph. Top: enlargement of region with archaeal lipids. Multiple peaks joined to a single molecular structure are diastereomers. Circles: *n*-alkanes. Squares: irregular acyclic isoprenoids.

Figure 5. Chromatograms illustrating contrasts between unmineralized (TI-94m, on left) and mineralized (OC-114m, on right) samples. Sat/Uns: hydrocarbon fraction of solvent extract. HPCH: hydrocarbon fraction of high-pressure, catalytic-hydrogenation products. (A, B) Selected-ion chromatogram for mass to charge ratio (*m/z*) 127, representing acyclic isoprenoids of archaeal origin. (C, D) Selected-ion chromatograms for *m/z* 191, representing tricyclic and pentacyclic terpanes, of bacterial origin. Squares designate tricyclic terpanes. Circles mark C_{29} and C_{30} 17α(H),21β(H) hopanes. Triangles indicate C_{31} to C_{35} extended hopanes.

References

1. Ueno, Y., Yamada, K., Yoshida, N., Maruyama, S. & Isozaki, Y. (2006) *Nature* **440,** 516-519.
2. Schidlowski, M., Hayes, J.M. & Kaplan, I. R. (1983) in *Earth's Earliest Biosphere: Its Origin and Evolution*, ed. Schopf, J. W. (Princeton University Press, Princeton. N.J.), pp. 149-186.
3. Eigenbrode, J. L. & Freeman, K. H. (2006) *Proc. Natl. Acad. Sci* **103,** 15759-15764.
4. Hayes, J. M. (1994) in *Nobel Symposium 84: Early Life on Earth*, ed. Bengtsen, S.
5. Kasting, J. F. (2005) *Precambian Res.* **137,** 119-129.
6. Sagan, C. & Mullen, G. (1972) *Science* **177,** 52-56.
7. Collister, J. W., Summons, R. E., Lichtfouse, E. & Hayes, J. M. (1991) *Org. Geochem.* **19,** 265-276.
8. Dix, G. R., Thomson, M. L., Longstaffe, F. J. & McNutt, R. H. (1995) *Precambrian Res.* **70,** 253-268.
9. De Rosa, M. & Gambacorta, A. (1988) *Prog. Lipid Res.* **27,** 153-175.
10. Chappe, B., Michaelis, W. & Albrecht, P. (1979) in *Advances in Organic Geochemistry 1979*, ed. Douglas, A. G., Maxwell, J.R. (Pergamon Press), pp. 265-274.
11. Carrillo-Hernandez, T. S., Adam, P., Albrecht, P., Derenne, S. & Largeau, C. (2001) in *21st International Meeting on Organic Geochemistry* (Krakow, Poland), p. 78.
12. Petrov, A. A., Vorobyova, N. S. & Zemskova, Z. K. (1990) *Adv. Org. Geochem.* **16,** 1001-1005.
13. Greenwood, P. F. & Summons, R. E. (2003) *Org. Geochem.* **34,** 1211-1222.
14. Buick, R., Rasmussen, B. & Krapez, B. (1998) *A.A.P.G. Bull.* **82,** 50-69.
15. Rasmussen, B. (2005) *Geology* **33,** 497-500.
16. Dutkiewicz, A., Rasmussen, B. & Buick, R. (1998) *Nature* **395,** 885-888.
17. Spangenberg, J. E. & Frimmel, H. E. (2001) *Chem. Geol.* **173,** 339-335.
18. Brocks, J. J., Logan, G. A., Buick, R. & Summons, R. E. (1999) *Science* **285**.
19. Lewan, M. D. (1997) *Geochim. Cosmochim. Acta* **61,** 3691-3723.
20. Jolly, W. T. (1978) *Geological Survey of Canada* **Paper 78-10,** 63-78.
21. Dimroth, E., Imreh, L., Rocheleau, M. & Goulet, N. (1982) *Can. J. Earth Sci.* **19,** 1729-1758.
22. Mycke, B., Michaelis, W. & Degens, E. T. (1988) *Org. Geochem.* **13,** 619-625.
23. Ayer, J. A., Ketchum, J. W. F. & Trowell, N. F. (2002) in *Summary of Field Work and Other Activities* (Ontario Geological Survey), pp. 5-1 to 5-16.
24. Brisbin, D. I. (1997) (Queen's University, Kingston, Ontario, Canada), p. 611.
25. Born, P. (1995) (Carleton University, Ottawa), p. 489.
26. Heaman, L. M. (1997) *Geology* **25,** 299-302.
27. Corfu, F., Jackson, S. L. & Sutcliffe, R. H. (1991) *Can. J. Earth Sci.* **28,** 489-503.
28. Bateman, R., Ayer, J. A., Barr, E., Dubé, B. & Hamilton, M. A. (2004) in *Discover Abitibi Initiative (41); Ontario Geological Survey, Open File Report 6145* (Queen's Printer for Ontario), p. 90.

29. Thompson, P. H. (2005) in *Discover Abitibi Initiative; Ontario Geological Survey, Open File Report 6162*, pp. 1-104.
30. Fyon, J. A., Crocket, J. H. & Schwarcz, H. P. (1983) *J. Geochem. Explor.* **18,** 245-266.
31. Veizer, J., Hoefs, J., Ridler, R. H., Jensen, L. S. & Lowe, D. R. (1989) *Geochim. Cosmochim. Acta* **53,** 845-857.
32. Gao, Z. L. & Kwak, T. A. P. (1997) *J. Geochem. Explor.* **59,** 259-274.
33. Craw, D. (2002) *Chem. Geol.* **191,** 257-275.
34. Jedwab, J. & Boulegue, J. (1984) *Nature* **310,** 41-43.
35. Sinninghe Damsté, J. S., Schouten, S., Hopmans, E. C., van Duin, A. C. T. & Geenevasen, J. A. J. (2002) *J. Lipid Res.* **43,** 1641-1651.
36. Montenegro, E., Gabler, B., Paradies, G., Seemann, M. & Helmchen, G. (2003) *Angew. Chem. Int. Ed.* **42**.
37. Maxwell, J. R., Cox, R. E., Eglinton, G., Pillinger, G. T., Ackman, R. G. & Hopper, S. N. (1973) *Geochim. Cosmoshim. Acta.* **37,** 297-313.
38. Patience, R. L., Rowland, S. J. & Mawxell, J. R. (1978) *Geochim. Cosmochim. Acta* **42,** 1871-1875.
39. Akhmedov, V. M., Al-Khowaiter, S. H., Akhmedov, E. & Sadikhov, A. (1999) *Appl. Catalysis A: General* **181,** 51-61.
40. Seewald, J. S. (1994) *Nature* **370,** 285-287.
41. Price, L. C. & DeWitt, E. (2001) *Geochim. Cosmochim. Acta* **65,** 3791-3826.
42. Summons, R. E., Brassel, S. C., Eglinton, G., Evans, E., Horodyski, R. J., Robins, N. & Ward, D. M. (1988) *Geochim. Cosmochim. Acta* **52,** 2625-2637.
43. Simoneit, B. R. T., Lein, A. Y., Peresypkin, V. I. & Osipov (2004) *Geochim. Cosmochim. Acta* **68,** 2275-2294.
44. Mycke, B. & Michaelis, W. eds. (1986a) *Molecular fossils from chemical degradation of macromolecular organic matter* (Pergamon Press, Oxford).
45. Grosjean, E. & Logan, G. A. (2007) *Org. Geochem.* **In Press**.
46. Oehler, J. H. (1977) *Precam. Res.* **4,** 221-227.
47. Behar, F. & Vandenbroucke, M. (1987) *Adv. Org. Geochem.* **13,** 927-938.
48. Kerrich, R. & Ludden, J. (2000) *Can. J. Earth Sci.* **37,** 135-164.
49. Loucks, R. R. & Mavrogenes, J. A. (1999) *Science* **284,** 2159-2163.
50. Huber, R., Huber, H. & Stetter, K. O. (2000) *Fems Microbiol. Rev.* **24,** 615-623.
51. Amend, J. P. & Shock, E. L. (2001) *FEMS Microbio. Rev.* **25,** 175-243.
52. Pedersen, K. (2000) *FEMS Microbiol. Lett.* **185,** 9-16.
53. Wellsbury, P., Mather, I. & Parkes, R. J. (2002) *FEMS Microbiol. Eco.* **42,** 59-70.
54. Bleeker, W. (1999) in *Economic Geology Monograph 10*, pp. 71-122.
55. Stefánsson, A. & Seward, T. M. (2003) *Geochim. Cosmochim. Acta* **67,** 1677-1688.
56. Gatellier, J.-P. & Disnar, J.-R. (1989) *Adv. Org. Geochem.* **16,** 631-640.
57. Peters, K. E., Walters, C. C. & Moldowan, J. M. (2005) *The Biomarker Guide* (Cambridge University Press).
58. Diessel, C. F. K., Brothers, R. N. & Black, P. M. (1978) *Contrib. Mineral. Petrol.* **68,** 63-78.
59. Holloway, J. R. (1984) *Geology* **12,** 455-458.

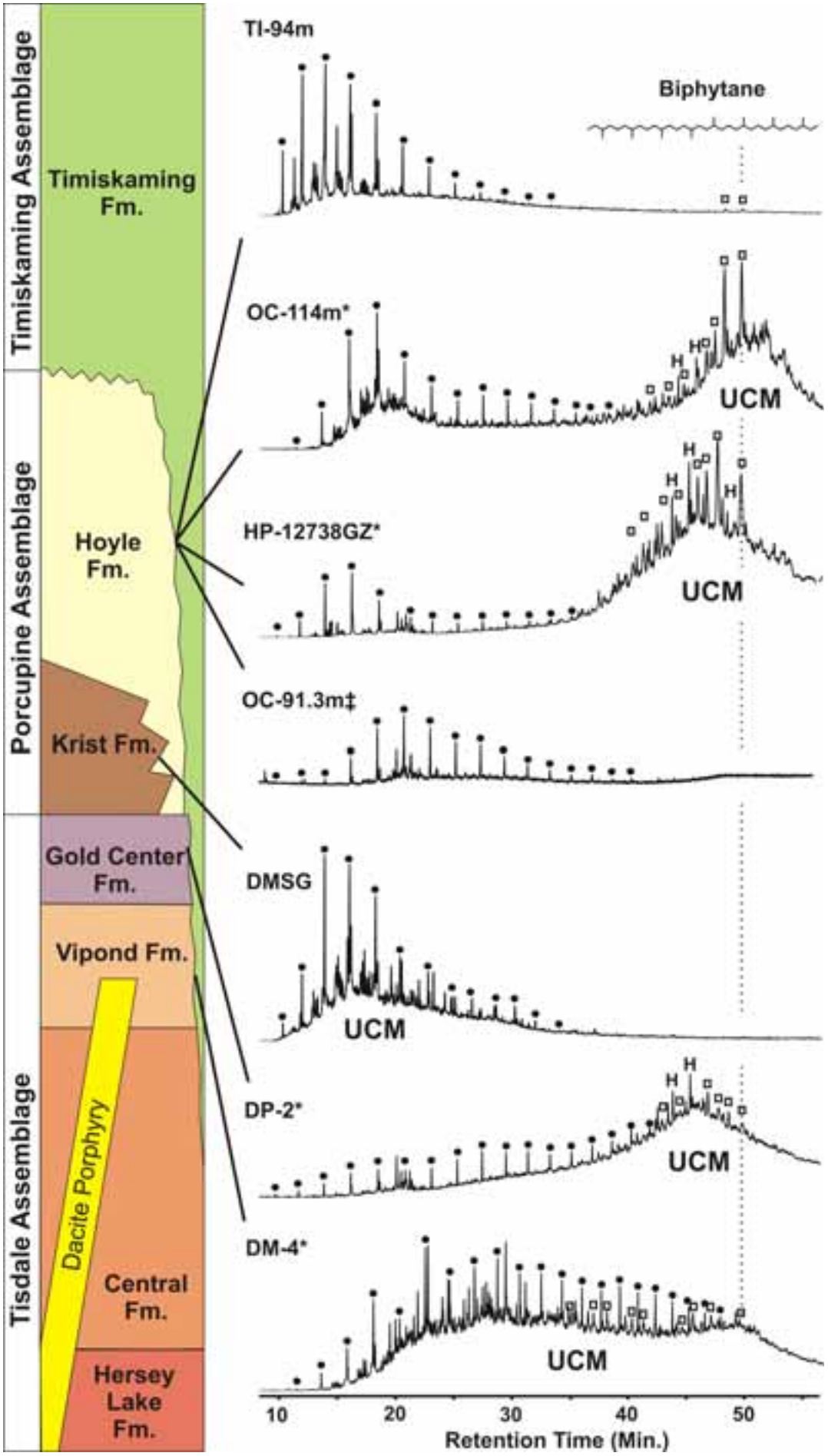
Timiskaming Assemblage
Timiskaming Fm.
Porcupine Assemblage
Hoyle Fm.
Krist Fm.
Tisdale Assemblage
Gold Center Fm.
Vipond Fm.
Dacite Porphyry
Central Fm.
Hersey Lake Fm.
TI-94m
Biphytane
OC-114m*
HP-12738GZ*
OC-91.3m‡
DMSG
DP-2*
DM-4*
UCM
H
10
20
30
40
50
Retention Time (Min.)

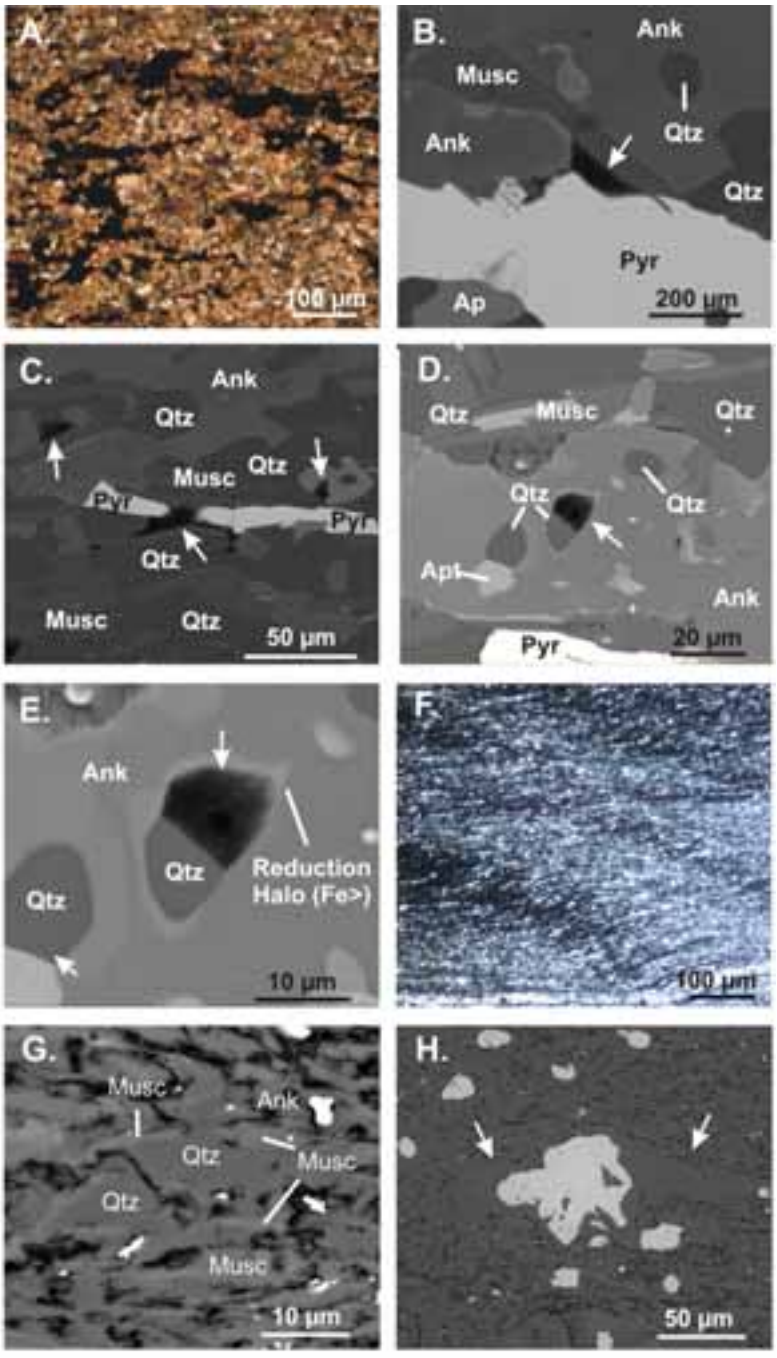
A.
100 µm
B.
Ank
Musc
Qtz
Ank
Qtz
Pyr
Ap
200 µm
C.
Ank
Qtz
Musc
Qtz
Pyr
Pyr
Qtz
Musc
Qtz
50 µm
D.
Qtz
Musc
Qtz
Qtz
Qtz
Apt
Ank
Pyr
20 µm
E.
Ank
Qtz
Reduction
Halo (Fe>)
Qtz
10 µm
F.
100 µm
G.
Musc
Ank
Qtz
Musc
Qtz
Musc
10 µm
H.
50 µm

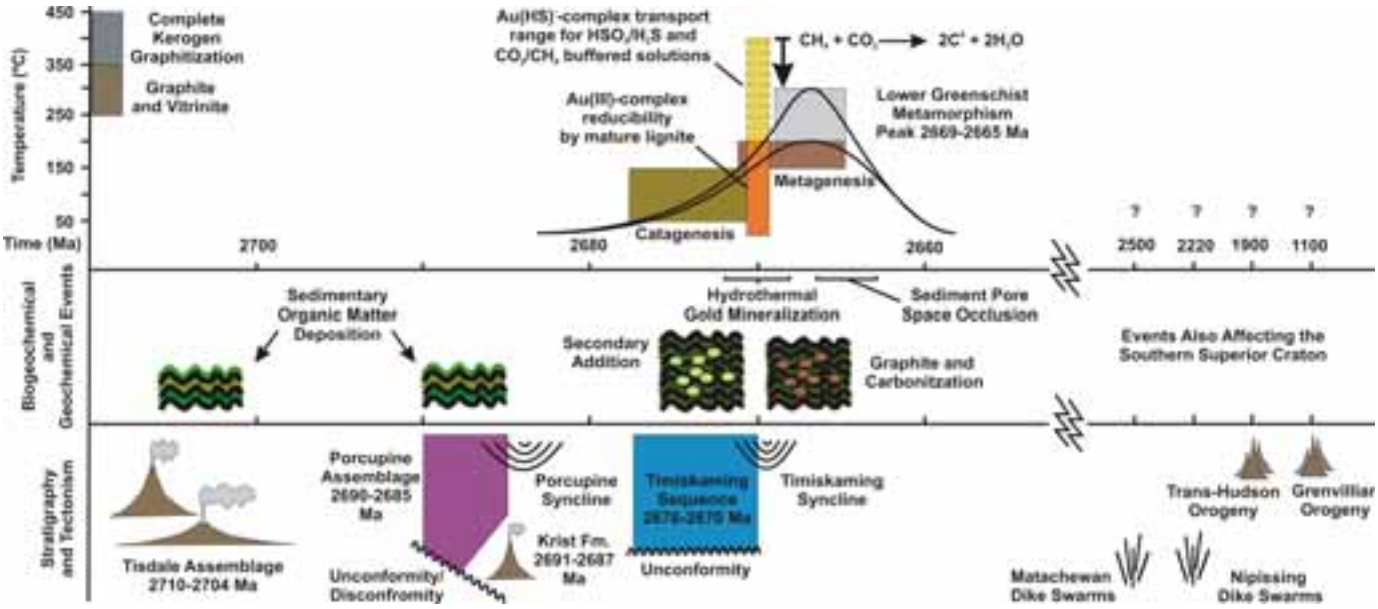
Temperature (°C)
450
350
250
150
50
Complete Kerogen Graphitization
Graphite and Vitrinite
Au(HS) -complex transport range for HSO4/H2S and CO2/CH4 buffered solutions
CH4 + CO2 → 2C0 + 2H2O
Au(III)-complex reducibility by mature lignite
Lower Greenschist Metamorphism Peak 2669-2665 Ma
Metagenesis
Catagenesis
Time (Ma)
2700
2680
2660
? ? ? ?
2500 2220 1900 1100
Biogeochemical and Geochemical Events
Sedimentary Organic Matter Deposition
Hydrothermal Gold Mineralization
Sediment Pore Space Occlusion
Secondary Addition
Graphite and Carbonitization
Events Also Affecting the Southern Superior Craton
Stratigraphy and Tectonism
Tisdale Assemblage 2710-2704 Ma
Porcupine Assemblage 2690-2685 Ma
Porcupine Syncline
Krist Fm. 2691-2687 Ma
Unconformity/ Disconfromity
Timiskaming Sequence 2676-2670 Ma
Timiskaming Syncline
Unconformity
Trans-Hudson Orogeny
Grenvillian Orogeny
Matachewan Dike Swarms
Nipissing Dike Swarms

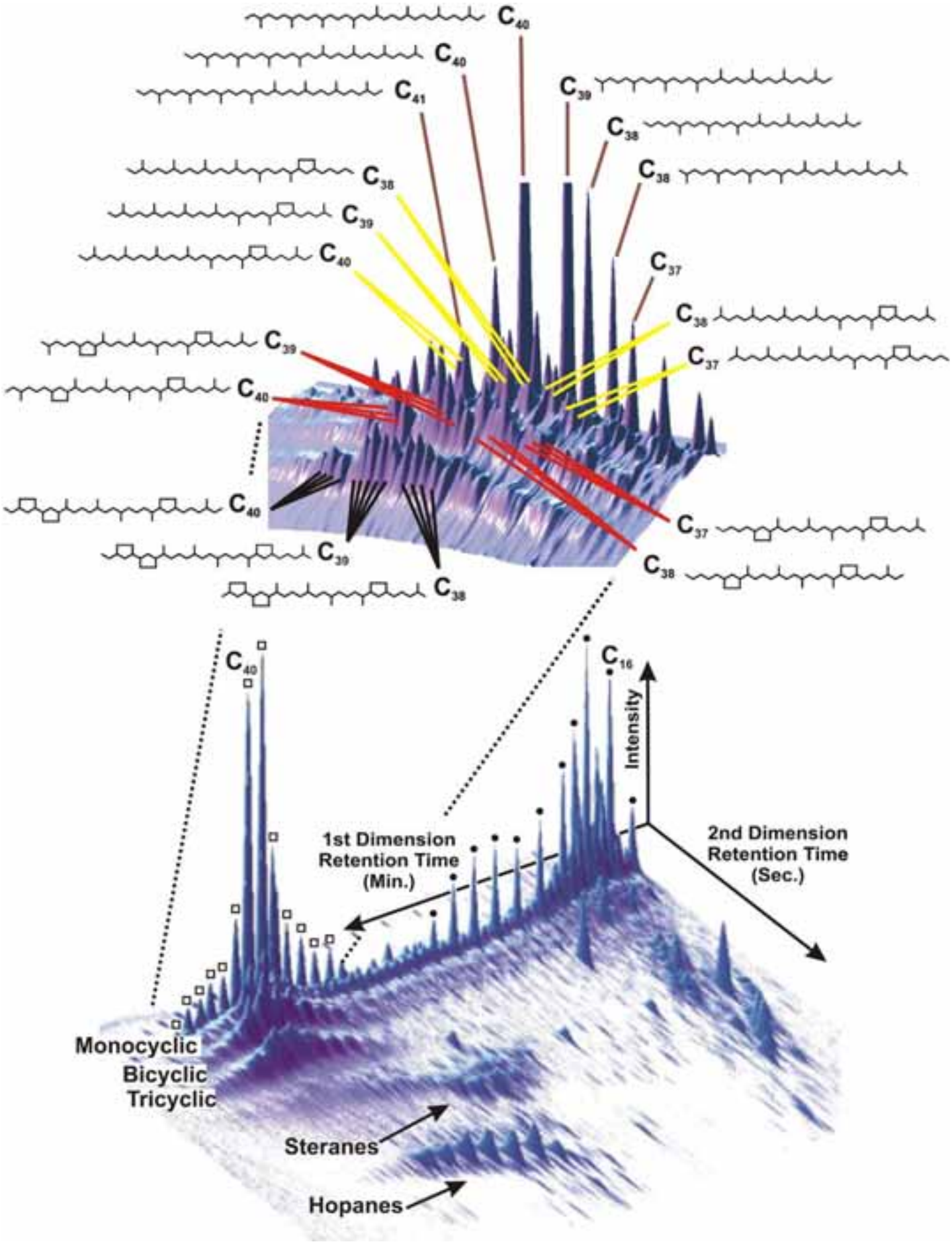
C40
C40
C41
C39
C38
C38
C38
C39
C40
C37
C38
C39
C37
C40
C40
C37
C39
C38
C38
C40
C16
Intensity
1st Dimension
Retention Time
(Min.)
2nd Dimension
Retention Time
(Sec.)
Monocyclic
Bicyclic
Tricyclic
Steranes
Hopanes

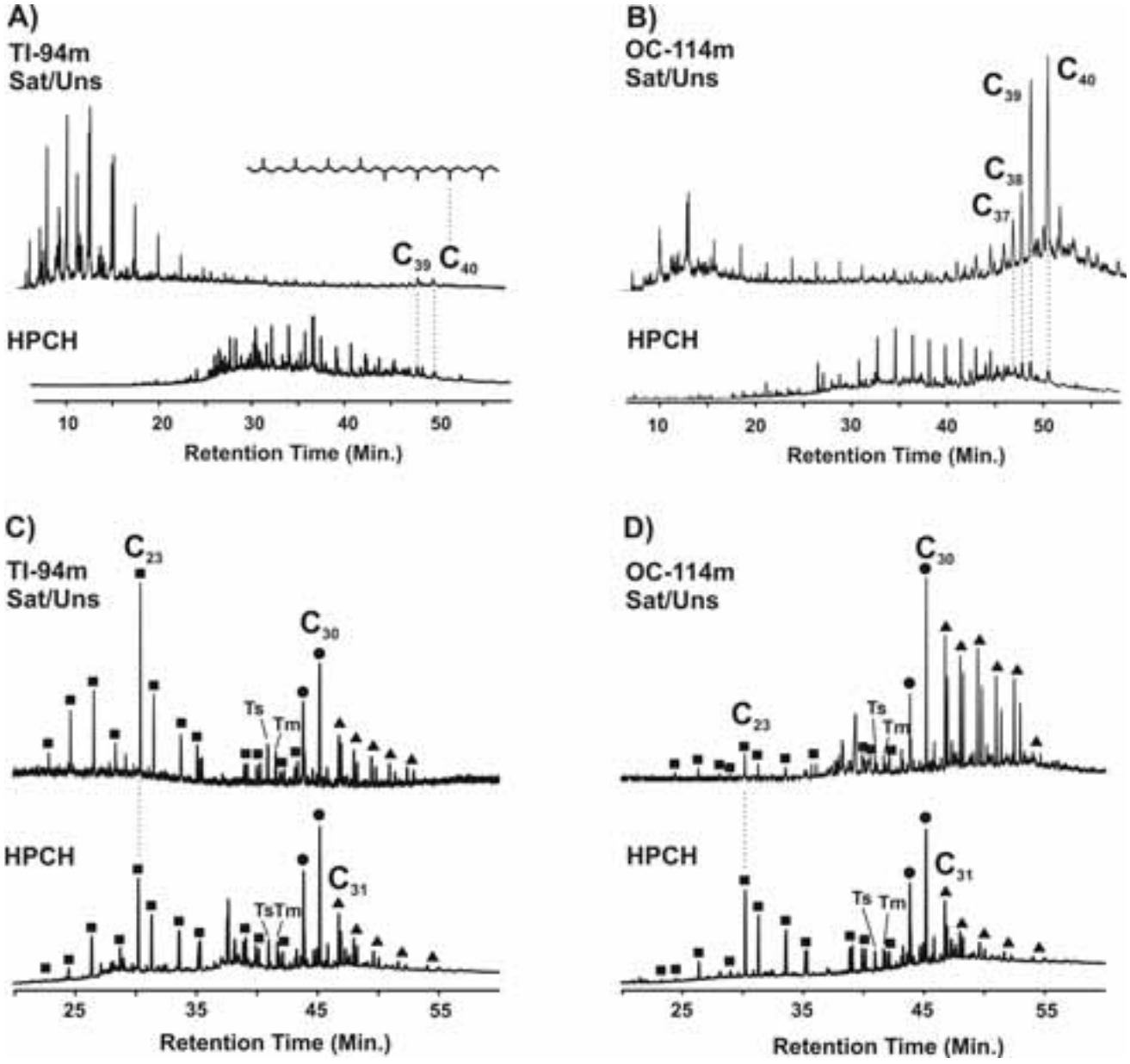
A)
TI-94m
Sat/Uns
C39 C40
HPCH
10
20
30
40
50
Retention Time (Min.)
B)
OC-114m
Sat/Uns
C39
C40
C38
C37
HPCH
10
20
30
40
50
Retention Time (Min.)
C)
TI-94m
Sat/Uns
C23
C30
Ts
Tm
HPCH
C31
TsTm
25
35
45
55
Retention Time (Min.)
D)
OC-114m
Sat/Uns
C30
C23
Ts
Tm
HPCH
C31
Ts Tm
25
35
45
55
Retention Time (Min.)

Table 1. Mass Yields, TOC, and $\delta^{13}C$

Sample Name	Mass (g)[1]	Bit (mg)[2]	s/u HC (ppm)[3]	Aro (ppm)[4]	TOC (Wt.%)[5]	C (g)[6]	H/C[7]	$\delta^{13}C_{VPDB}$ (‰)[8]
Hoyle Formation								
TI-94m	141.93	49.0	23.3	2.1	2.0	2.8	0.020	-39.1
TI-117.8m	130.82	12.0	0.3	15.3	0.9	1.2	0.019	-31.7
TI-82.5m	120.28	16.0	34.9	15.8	0.8	1.0	0.087	-33.7
TI-83m	134.84	10.0	17.1	4.4	1.8	2.4	0.128	-33.7
TI-275.14m	63.08	30.0	28.5	46.0	5.1	3.2	0.003	-42.0
TI-52m	95.81	37.0	4.2	1.0	3.7	3.5	0.012	-36.6
TI-180m	130.81	1.0	0.3	24.5	1.1	1.4	0.029	-29.7
TI-603m	109.37	4.0	7.3	2.7	0.4	0.4	0.041	-29.2
TI-39.25m	131.58	7.0	0.8	2.3	0.4	0.5	0.006	-21.5
TI-128.75m	123.66	1.0	0.8	1.6	0.2	0.2	Nm	-20.9
OC1-114m	104.08	16.0	2.9	0.4	9.3	4.7	0.005	-28.7
OC1-118m	157.91	8.0	0.3	0.3	4.5	7.1	0.005	-28.5
OC1-116.5m	43.27	4.0	18.5	4.6	4.6	2.0	0.000	-33.7
OC1-161.7m	75.37	24.0	13.3	91.5	4.9	3.7	0.000	-31.6
OC-89m	121.06	3.0	8.3	0.8	1.2	1.5	0.011	-25.4
OC-110.8m	51.37	3.0	77.9	1.9	7.4	3.8	0.000	-34.8
HP12687	42.07	1.0	28.5	0.4	1.0	0.4	0.003	-19.5
Grey Zone Samples								
HP12738 GZ	61.59	1.0	28.5	4.8	1.2	0.6	0.007	-37.2
HPGZ-2	89.51	0.6	6.5	4.9	Nm	Nm	Nm	Nm
Basalt Units								
OC-91.3m	41.0	0.2	4.9	Nm	Nm	Nm	Nm	Nm
OC-49.2m	63.57	0.5	3.1	Nm	Nm	Nm	Nm	Nm
OC-147.5m	52.59	0.15	1.9	Nm	Nm	Nm	Nm	Nm
OC-153m	61.13	0.2	3.3	Nm	Nm	Nm	Nm	Nm
Krist Formation								
DMGS	161.5	10.0	8.7	1.9	1.7	2.8	0.013	-20.9
Gold Center Formation								
DP-1	143.33	10.0	0.2	0.2	0.4	0.5	0.035	-16
DP-2	99.06	1.0	0.04	0.04	0.1	0.1	0.013	-15.1
Vipond Formation								
DM-1	173.43	5.0	0.2	0.2	0.6	1.1	0.021	-15.7
DM -2	127.18	25.0	0.9	0.4	0.5	0.7	0.008	-32.5
DM -3	183.83	1.0	0.3	0.04	0.1	0.1	0.040	-27.3
DM -4	158.84	6.0	0.2	0.1	0.1	0.1	0.000	-28.8

[1] Mass of ground rock powder used in solvent-extraction.
[2] Mass of extracted bitumen.
[3] s/u HC (ppm) = parts per million (ppm) hydrocarbon fraction calculated 1 µg hydrocarbons/gram rock powder.
[4] Aro = aromatic hydrocarbon fractions in parts ppm.
[5] TOC = total organic carbon measured as weight percent of kerogen per mass of extracted rock powder.
[6] C = grams of carbon is mass of solvent-extracted rock powder multiplied by TOC.
[7] H/C = hydrocarbon/carbon ratio of the kerogen.
[8] Carbon isotopic values *vs* VPDB in ‰ notation from non-extracted rock powder.
Nm: Parameter not measured.